Semitransparent Poly(styrene-*r*-maleic anhydride)/ Alumina Nanocomposites for Optical Applications

Alexander Chandra,[1] Lih-Sheng Turng,[1] Padma Gopalan,[2] Roger M. Rowell,[3] Shaoqin Gong[4]

[1]*Polymer Engineering Center, Department of Mechanical Engineering, University of Wisconsin at Madison, Madison, Wisconsin 53706*
[2]*Materials Science and Engineering, University of Wisconsin at Madison, Madison, Wisconsin 53706*
[3]*Forest Products Laboratory, Forest Services, U.S. Department of Agriculture, Madison, Wisconsin 53726*
[4]*Department of Mechanical Engineering, University of Wisconsin at Milwaukee, Milwaukee, Wisconsin 53211*

Received 8 November 2006; accepted 8 February 2007
DOI 10.1002/app.26349
Published online 14 May 2007 in Wiley InterScience (www.interscience.wiley.com).

ABSTRACT: This article presents the development and characterization of transparent poly(styrene-*r*-maleic anhydride) (SMA)/alumina nanocomposites for potential use in optical applications. Chemically treated spherical alumina nanoparticles were dispersed in an SMA matrix polymer via the solution and melt-compounding methods to produce 2 wt % nanocomposites. Field emission scanning electron microscopy was used to examine the nanoparticle dispersion. When the solution method was used, nanoparticle reagglomeration occurred, despite the fairly good polymer wetting. However, through the coating of the alumina nanoparticles with a thin layer (ca. 20 nm) of low-molecular-weight SMA, reagglomeration was absent in the melt-compounded samples, and this resulted in excellent nanoparticle dispersion. The resultant nanocomposites were semitransparent to visible light at a 2-mm thickness with improved UV-barrier properties. Their impact strengths, tensile strengths, and strains at break were slightly reduced compared with those of their neat resin counterpart, whereas a small enhancement in their moduli was achieved. © 2007 Wiley Periodicals, Inc. J Appl Polym Sci 105: 2728–2736, 2007

Key words: nanocomposites; nanotechnology; UV-vis spectroscopy

INTRODUCTION

Polymer nanocomposites, which consist of a polymer matrix filled with nanosize particles ranging from 0.5 to 100 nm in size, represent a new class of lightweight, high-performance materials that exhibit improved tensile strength, heat resistance, barrier properties, and flame retardation and have found commercial applications (e.g., polymer-layered silicate clay nanocomposites for automotive components). Research on polymer nanocomposites has exploded in recent years because of the tremendous number of potential applications.[1] However, there has been very little focus on the study of non-silicate-layer-based, transparent nanocomposites, especially those that use the melt-compounding method, which could potentially impact a broad range of industrial sectors, including aerospace, automotive, construction, consumer electronic, electrical, food packaging, health, medical, military, ophthalmic, optical, optoelectronic, and photonic industries. For that reason, we have aimed in this study to develop and characterize new nanocomposites that can replace neat polymer resins or glass in various optical applications. The idea is to incorporate chemically treated spherical nanoparticles of the proper size (much smaller than the visible-light spectrum) and attributes (e.g., UV absorption or a high refractive index) into the polymer matrix and disperse them at the nanoscale to minimize light scattering and attain optical transparency while realizing the retention of or improvements in some of the optical and material properties, such as tribological properties, mechanical properties, dimensional stability, and UV-barrier properties.

The interface between an inorganic nanoparticle and the polymer host is a crucial factor that needs to be taken into account when optimum polymer/nanoparticle composites are being created. This interface dictates desirable nanocomposite properties such as nanoparticle dispersion as well as nanocomposite strength, toughness, and optical clarity. The interface consists of two essential elements, namely, the bonding between the nanoparticle and the coupling agent and the bonding between the coupling agent and the polymer host. Therefore, one strategy would be to provide a covalent link between the polymer host, the coupling agent, and the nanoparticle.

Correspondence to: L.-S. Turng (turng@engr.wisc.edu).
Contract grant sponsor: Essilor of America, Inc. (through the Polymer Engineering Center Industrial Consortium).
Contract grant sponsor: University of Wisconsin at Madison (through a Madison Graduate School Industrial and Economic Development Research award).

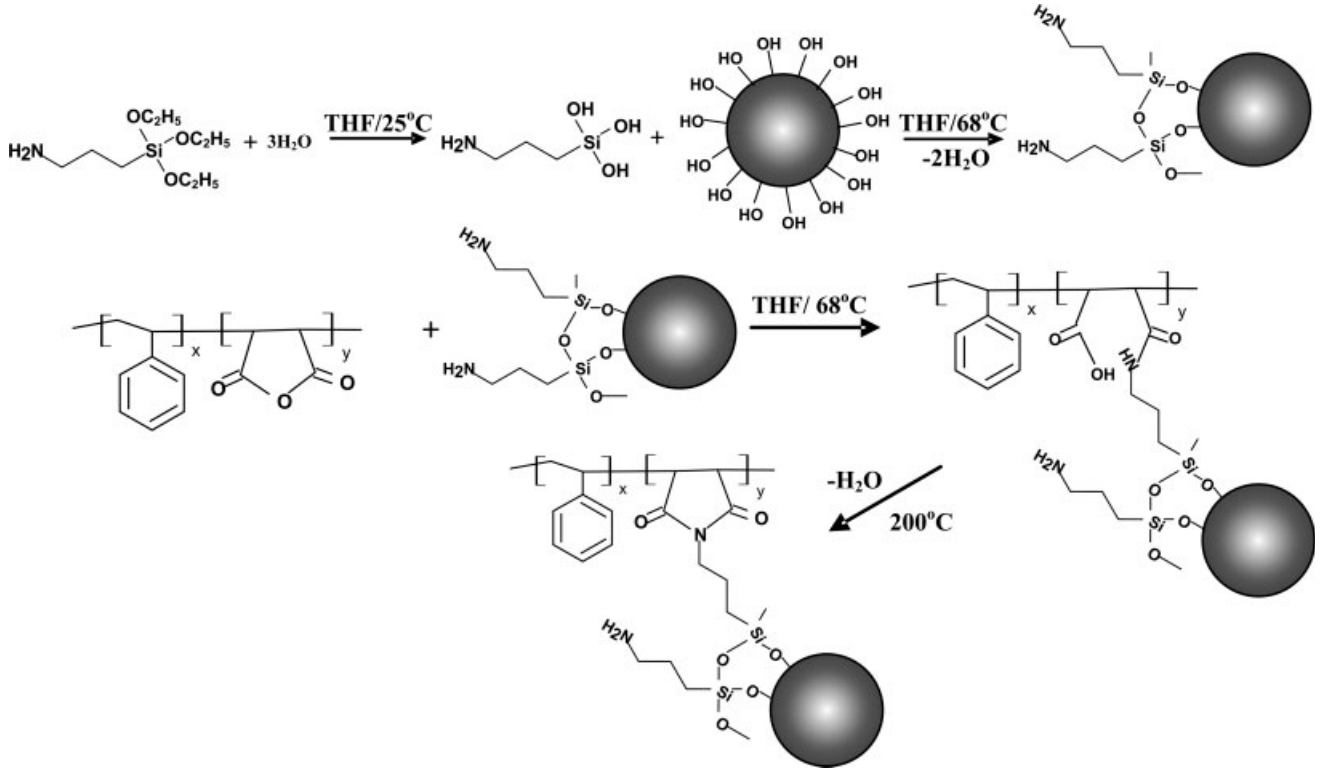

Figure 1 Reaction scheme of the nanoparticles covalently bonded with the polymer host.

This is often difficult as the appropriate functional groups need to be in the thermoplastic host to bring about the chemical reaction with the coupling agent. For optical applications, one of the transparent thermoplastics with reactive groups is the copolymer poly(styrene-*r*-maleic anhydride) (SMA), with maleic anhydride serving as reactive sites that can be easily reacted with amine groups, creating imide bonds, as depicted in Figure 1.[2] Furthermore, one type of spherical nanoparticle that can be potentially used for optical nanocomposites is the alumina nanoparticle, and the hydroxide groups on the nanoparticle surface can be covalently coupled with SMA by the use of an aminosilane coupling agent.

Another method of facilitating the dispersion of nanoparticles is to coat the nanoparticles with a thin layer of a polymer to introduce steric stabilization.[3] Through the coating of the nanoparticle surface with a thin layer of a polymer, the strong van der Waals influence from the nanoparticles can be masked, and this prevents particle agglomeration. The resulting core/shell nanohybrids can then be easily compounded with the host polymer to fabricate nanocomposites. The interface between the nanoparticles and the polymer coating is important, and the best strategy for this would be to have covalent bonding on the nanoparticle surface. The covalent bond with the polymer coating would ensure a proper and well-adhered coating on the nanoparticle surface. Low-molecular-weight SMA is a potential candidate for such coatings in which primary amines commonly available in organosilane coupling agents can react with the maleic anhydride groups. Furthermore, because it is transparent to visible light and its refractive index of 1.583 is in the proximity of several other optically clear polymers (e.g., polycarbonates), it will not hamper the overall transparency of the host materials.

Therefore, this study has been aimed at producing transparent nanocomposites with commercially available materials via the solution method to ensure complete wetting between the nanoparticles, the coupling agent, and the polymer matrix, thus optimizing the direct covalent bonding between the polymer host and the nanoparticles. In addition, the same approach was used to coat the alumina nanoparticles with a thin layer of low-molecular-weight SMA from which the nanoparticles could be blended easily with the melt-compounding method (a high-intensity batch mixer was used in this study). Compared with the solution method, melt compounding is more advantageous for mass production. Melt compounding would allow the existing mixing/compounding equipment, such as extruders or batch mixers, to be used and hence could be easily scaled up for commercial production. Nanoparticle dispersions are reported in this article together with the resulting light transmittance, UV-barrier properties, and mechanical

properties of the nanocomposites, such as the tensile properties and impact strength.

EXPERIMENTAL

Materials

SMA copolymers were obtained from Sartomer (Exton, PA) and NOVA Chemicals (Moon Township, PA). The SMA EF-80 (weight-average molecular weight = 14,400, glass-transition temperature = 104°C) from Sartomer was a low-molecular-weight copolymer with an 8 : 1 molar ratio of styrene to maleic anhydride, whereas the high-molecular-weight SMA copolymer (melt flow index = 2 g/10 min) from NOVA Chemicals had proprietary molecular weight and composition information. The alumina nanoparticles with an average particle diameter (D_{50}) of 96 nm and an average specific surface area of 50.4 m^2/gm were purchased from Nanotechnologies, Inc. (Austin, TX). Fluorescamine and the aminosilane coupling agent 3-aminopropyltriethoxysilane (weight-average molecular weight = 221.4 g/mol, specific surface area = 353 m^2/g) were purchased from Sigma–Aldrich (St. Louis, MO) and Gelest, Inc. (Morrisville, PA), respectively, and all chemicals were used as received without further purification.

Coupling agent treatment

The alumina nanoparticles were dried at 100°C under a vacuum overnight, and this was followed by the dispersion of 5 wt % alumina nanoparticles through ultrasonic vibrations in tetrahydrofuran (THF) for 10 min to break up any agglomerates. At the same time, the required coupling agent was calculated on the basis of the specific surface areas of both the nanoparticles and the coupling agent, and a 30 wt % excess of the aminosilane coupling agent was prehydrolyzed with a 1 : 3 molar ratio of deionized water (so that there was 3 mol of water for every mole of aminosilane) in a small amount of THF for 3 min. The prehydrolyzed coupling agent was then added dropwise to the alumina nanoparticle solution in a water bath at room temperature under constant ultrasonic vibration for 15 min. Afterwards, the nanoparticle solution was quenched with an equal amount of THF to slow the reaction, and the nanoparticles were separated by centrifugation at 1000 rpm for 6 min. After the removal of the supernatant, fresh THF was added to the separated nanoparticles to remove any excess coupling agent, and this washing process was repeated twice. Finally, fresh THF was added to the treated nanoparticles to reach a 5 wt % concentration, and the solution was refluxed overnight.

Fluorescamine was used as a qualitative check to examine if the treatment was successful. By the addition of a small amount (<0.5 mg) of fluorescamine to approximately 1 mg of the treated nanoparticles in 1.5 mL of acetone, a reaction with the primary amine (NH_2 from the coupling agent) occurred, resulting in a compound that fluoresced under UV light.[4] It was found that 15 min was sufficient for this treatment as demonstrated by the fluorescent reaction of alumina nanoparticles (which turned light yellow) after multiple washing steps with a fresh solvent, sonication, and UV-light exposure, as shown in Figure 2. This suggests that the aminosilane coupling agent covalently bonded with the alumina nanoparticles. Untreated alumina nanoparticles after fluorescamine and UV exposure are also shown in Figure 2 for comparison.

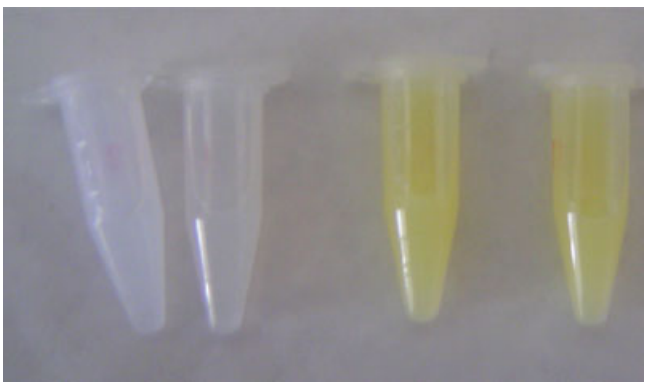

Figure 2 Fluorescent reaction (yellowing) of the treated alumina nanoparticles dispersed in THF after UV-light exposure. [Color figure can be viewed in the online issue, which is available at www.interscience.wiley.com.]

Polymer coating over nanoparticles

The THF from the refluxed nanoparticle solution (aminosilane-treated) was separated by centrifugation, and fresh THF was added. Separately, 0.1% (w/v) of the low-molecular-weight SMA EF-80 was dissolved in THF, and the treated nanoparticles were added dropwise under rigorous stirring into the polymer solution to reach a 1% (w/v) concentration; this was followed by sonication of the solution for 15 min. Afterwards, the solution was refluxed for 3 h, and this was followed by similar washing by the centrifugation process at 3500 rpm for 20 min three times on the coated nanoparticles. The final supernatant from the washed nanoparticles was tested for any unbound polymer through mixing with water. The coated alumina nanoparticles were collected only when there was no excess polymer precipitated in the water. Finally, the separated alumina nanoparticles were dried at 90°C under a vacuum overnight and stored for future use. Figure 3 shows the energy filtered transmission electron microscopy (EFTEM) image of the polymer coating on the alumina

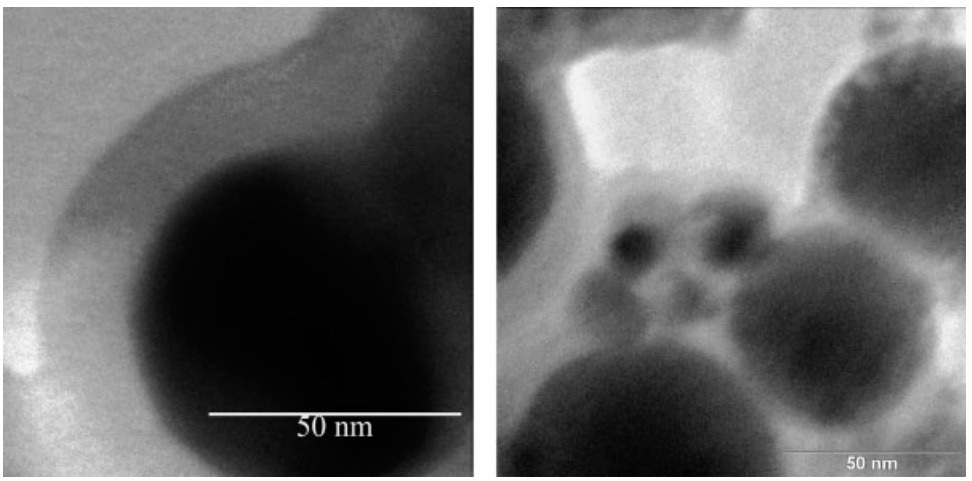

Figure 3 EFTEM micrographs of the SMA EF-80 polymer coated alumina nanoparticles.

nanoparticles. The SMA was found to be uniformly coated on the surface of the individual alumina nanoparticles and was approximately 20 nm thick.

Polymer nanocomposite from the solution method

The THF from the refluxed nanoparticle solution (aminosilane treatment) was removed by centrifugation, and fresh THF was added. Separately, 10% (w/v) of the high-molecular-weight SMA was dissolved in THF, and the aminosilane-treated nanoparticles were added dropwise to a small aliquot of the SMA–THF solution under rigorous stirring. Afterwards, the well-stirred mixture was sonicated for 15 min and added to the remaining SMA–THF solution to form a final concentration of 2 wt % alumina in SMA; this was followed by additional sonication of the solution for 1 min. In this study, the sonication time was limited to 15 min to minimize the degradation of polymer molecules and yet achieve fairly uniform nanoparticle dispersion. After the sonication process, the solution was refluxed for 3 h under rigorous stirring. Separately, the same steps were performed for the SMA neat resin to exclude the effects of polymer degradation from the ultrasonic vibration. Finally, the SMA nanoparticle blend and the SMA neat resin were precipitated in isopropyl alcohol and dried at 90°C under a vacuum overnight; this was followed by vacuum-oven drying at 200°C for 10 min to complete the imide conversion.

Polymer nanocomposite from the thermokinetic mixer

The thermokinetic mixer (K-mixer) is a unique batch mixer because it does not possess any external heating elements. All the heat required to melt the polymer is achieved from the friction between the mixing elements, the polymer, and the surrounding wall when the nanoparticles and the polymers are processed (at 5000 rpm in this case). The polymer-coated alumina nanoparticles were first hand-mixed with the polymer pellets into a 2 wt % loading, and this was followed by compounding until a release temperature of $\sim$ 227°C. The resulting hot nanocomposites were then pressed into plates and pelletized. Again, to exclude the degradation effects from compounding, the dry SMA neat resin was processed similarly and tested for comparison.

Sample preparation and characterization

The dried, precipitated, and melt-compounded nanocomposites were hot-pressed with a Carver press (Menomonee Falls, WI) at 204°C into 2-mm-thick rectangular shapes from which 50 mm $\times$ 12 mm $\times$ 2 mm rectangular bars with a 2-mm notch were machined. At the same time, only the precipitated nanocomposite and its neat resin counterparts were injection-molded into tensile bar specimens with a Haake Minijet desktop injection-molding instrument (Waltham, MA). A Hitachi U-3010 UV–vis spectrophotometer (Hitachi Instruments, San Jose, CA) was employed to measure the light transmittance with wavelengths ranging from 280 to 700 nm, whereas a Leo 1530 field emission scanning electron microscope (Peabody, MA) at a 3-kV acceleration voltage was used to investigate the nanoparticle dispersion on the freeze-fractured nanocomposite surfaces. In addition, a Leo 912 energy filtered transmission electron microscope (Peabody, MA) was used to investigate the resulting polymer coating on the nanoparticles. Finally, a standard ASTM D 256 Izod impact test and an ASTM D 638 tensile test were performed on the samples. An MTS Sintech 10/GL (MTS, Eden Prairie, MN) was used to measure the tensile proper-

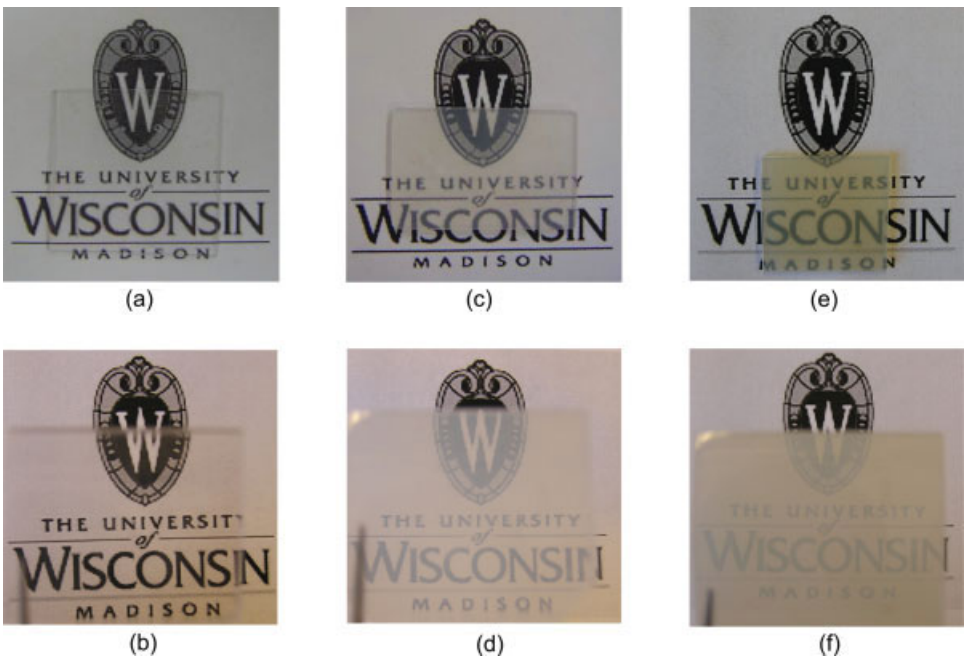

Figure 4 Qualitative transparency of the SMA neat resin and its nanocomposite samples: (a) SMA neat resin, (b) SMA neat resin held 12 cm above the background image, (c) SMA/2 wt % alumina nanocomposite from the solution method, (d) SMA/2 wt % alumina nanocomposite from the solution method held 12 cm above the background image, (e) SMA/2 wt % alumina nanocomposite from the melt-compounding method, and (f) SMA/2 wt % alumina nanocomposite from the melt-compounding method held 12 cm above the background image. The sample thickness was 2.0 mm. [Color figure can be viewed in the online issue, which is available at www.interscience.wiley.com.]

ties of the injection-molded specimens at a strain rate of 5.08 mm/min. Three to five specimens were used for each mechanical test.

RESULTS AND DISCUSSION

Nanocomposite light transmittance and dispersion

The transparency of the high-molecular-weight SMA neat resin and its nanocomposite samples is shown in Figure 4, with their visible-light-transmittance spectra shown in Figure 5. Each light-transmittance sample was 2 mm thick, and the samples were polished to remove any surface imperfections that would otherwise have affected their light scattering behavior. Currently, only the light transmittance of the nanocomposites and their near resin counterparts was measured, although the transmission haze is another important property for optical products to be measured in future studies. The haze is a measure of how much light is scattered by the media.

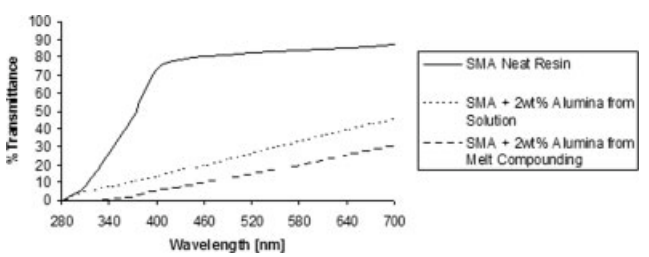

Figure 5 Visible-light transmittance of the SMA neat resin and its nanocomposite.

As shown in Figure 5, the visible-light transmittance of the nanocomposites was reduced, especially at shorter wavelengths. The D_{50} diameter of the alumina nanoparticles used in this study was 96 nm, and on the basis of Raleigh scattering, dramatic light-transmittance loss can be avoided when the nanoparticle size is kept below 30 nm.[5] The light scattering behavior is also affected by the incident wavelength.[6] This can be observed in Figure 5, in which the light-transmittance losses are more pronounced at shorter wavelengths because the nanoparticle size is closer in comparison with the wavelengths. Apart from the light scattering, the nanoparticles might possess some degree of light absorption, and a mismatch of the refractive indices between the SMA matrix and alumina nanoparticles might further decrease the overall nanocomposite transparency. To further discuss the resulting light transmittance, the nanoparticle dispersion of the nanocomposites is shown in Figure 6. In the nanocomposites produced with the solution method, the individual spherical nanoparticles in the agglomerates were harder to distinguish, and their surface appeared rough. Such roughness was caused by the SMA layer coated on the surface of the agglomerates, which ultimately affected the secondary emission as

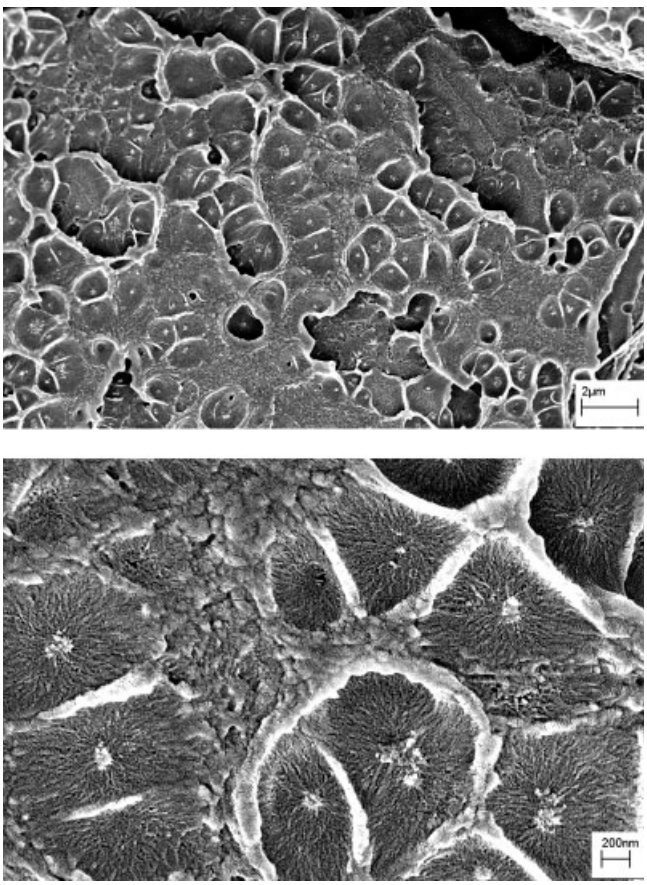

Figure 6 FESEM micrographs of SMA/2 wt % alumina nanocomposites from the solution method.

detected by field emission scanning electron microscopy (FESEM). Because the nanocomposites were produced via the solution method, better wetting was allowed by the polymer onto the nanoparticle surfaces. In addition, it was further enhanced by the primary amine reactive sites on the nanoparticle surface. Such enhancements could also be observed from the lack of voids on the freeze-fractured surface. Voids are usually caused by debonding between the nanoparticles and the polymer matrix where the interactions between the two are weak.

One particular drawback of using the solution method for the SMA/alumina nanocomposite can be observed by a small amount of the still large agglomerates (200 nm or larger) at different locations. Although the majority of the nanoparticle agglomerates were smaller, the few larger agglomerates suggest that there was a nonuniform size distribution in the nanoparticle agglomerates. These large agglomerates exacerbated the light scattering behavior, thus reducing the overall light transmittance. During precipitation, the process had to be performed slowly to prevent the formation of glutinous precipitates because the THF solvent could not be extracted fast enough from the polymer. Furthermore, only mechanical stirring was performed during precipitation because excessive sonication would have resulted in further polymer degradation.[7,8] This absence of adequate force to separate the nanoparticles eventually caused reagglomeration. In addition, the presence of isopropyl alcohol might introduce the poor-solvent effect, which could also induce reagglomeration.[3] In a poor solvent, the polymer molecules on the nanoparticle surface try to squeeze the solvent away. Therefore, the nanoparticles are further compressed together, promoting reagglomeration. Finally, the larger molecular weight SMA on the nanoparticle surface may entangle or bridge multiple nanoparticles together, hence creating agglomerates that are harder to separate.[3]

Figure 7 shows that the nanoparticle dispersion on the nanocomposite compounded with the K-mixer was better. A close examination over a large area of the freeze-fractured surface found no large agglomerates, and it appeared that the nanoparticles were dispersed to their individual elements because their size was close to the nanoparticle D_{50} value of 96 nm. This was because the K-mixer is a highly aggressive compounder capable of rotating at 5000 rpm and the nanoparticles were coated with a low-

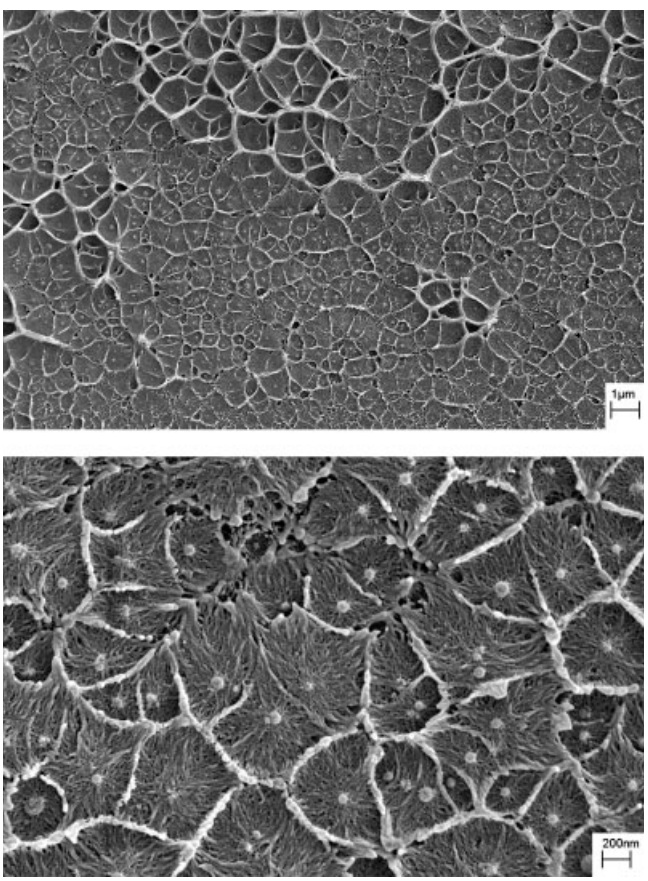

Figure 7 FESEM micrographs of SMA/2 wt % alumina (SMA EF-80 coated) nanocomposites from the K-mixer.

molecular-weight polymer, which further masked the strong van der Waals attraction. During compounding, the materials experienced intense shear between the mixing elements and the surrounding wall. Once the friction and shear heating had softened the melt, it was subjected to more shear and elongational force by the mixing elements until the release temperature of the polymer melt was achieved.

Although the melt-compounded nanocomposite showed better nanoparticle dispersion, its light transmittance was surprisingly lower than that of the nanocomposite produced via the solution method. The reason for the lower light transmittance of the better dispersed, melt-compounded nanocomposite is unknown and requires further research. However, the freeze-fractured surface of the SMA nanocomposites showed multiple craters surrounding the nanoparticle agglomerates. It is not yet understood why such fractured surfaces were formed, but these craters appeared to be the interfacial regions that were present as a result of the more compatible surfaces between the nanoparticles and the SMA host polymer. Nonetheless, these craterlike regions surrounding the nanoparticles may affect the light scattering effect and thus further decrease nanocomposite transparency. Additionally, the improved nanoparticle dispersion provided even more scattering sites, as the nanoparticle average diameter of 96 nm was not small enough to minimize light scattering, which further exacerbated overall light scattering.

The nanocomposites also demonstrated improved UV-light-barrier characteristics. UV radiation from the sun falls within the range of 280–380 nm. As shown in Figure 5, the UV-light transmittance of the SMA nanocomposites fell far below that of the neat resin. Metal oxide nanoparticles are generally capable of absorbing UV light, and their activity is material- and crystal-phase-dependent.[9–11] However, at the same time that the UV light is absorbed at the surface, an electron is promoted to the conduction band, thus leaving an electron hole in the valence band. Both the reactive electron and the electron hole can travel to the surface and react with oxygen and hydroxide ions to form reactive ·OH radicals. Such radicals induce polymer degradation by initiating random chain scissions in the host polymer; this is also known as photocatalytic degradation.[12,13] Excessive chain scissions lower the host polymer molecular weight, thus decreasing their mechanical properties. Hence, the choice of nanoparticles and the host polymer is important so that UV-barrier properties can be improved while the degradation induced by the nanoparticle is minimized. On the basis of the very slight discoloration of the nanocomposite, the alumina nanoparticles used in this study were not as reactive as anatase titanium dioxide reported previously.[9] Furthermore, the coupling agent and the thin polymer coating on the nanoparticles prevented direct contact with the host matrix, thereby lessening the degradation.

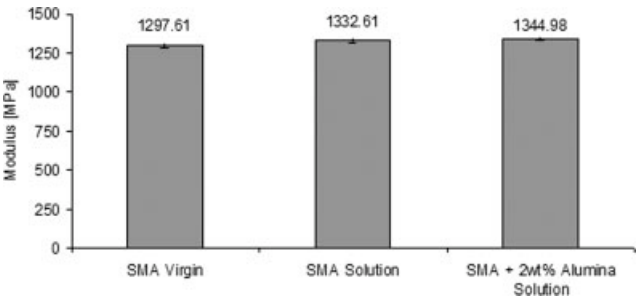

Figure 9 Moduli of the SMA neat resins and their nanocomposite counterparts from the solution method.

Mechanical properties

The tensile and impact properties of the SMA alumina nanocomposites and their neat resins are shown in Figures 8–11. Because of the limited amount of materials, the tensile tests were performed only on the solution-method systems. As shown in all the figures, the nanocomposites did not show improvements except in their modulus, for which there was a slight increase. In addition, the

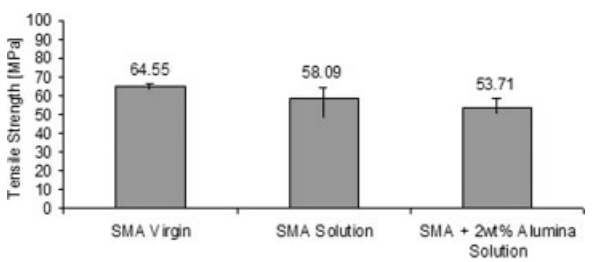

Figure 8 Tensile strengths of the SMA neat resins and their nanocomposite counterparts from the solution method.

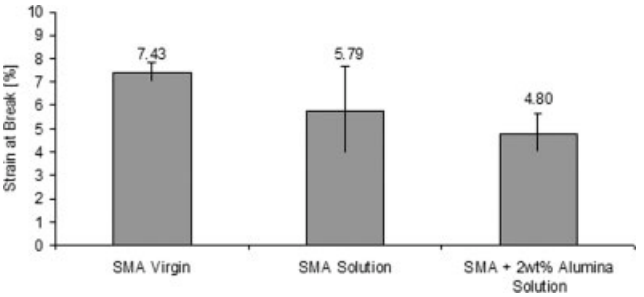

Figure 10 Strains at break of the SMA neat resins and their nanocomposite counterparts from the solution method.

precipitated neat resin also demonstrated a higher modulus, a lower tensile strength, a lower strain at break, and a lower impact strength than the virgin neat resin.

The commercial virgin SMA copolymer might have contained additives that were dissolved and removed during the precipitation process, thus affecting the overall mechanical properties. Moreover, a prolonged sonication process performed on the neat resin might have degraded the polymer by chain scission, resulting in shorter and lower molecular weight chains.

At the beginning, it was postulated that the mechanical properties of nanocomposites could be improved if we took advantage of direct covalent bonding between the nanoparticle and the polymer matrix. However, it is evident that no significant improvements in the mechanical properties were achieved through this method. Thio et al.[14] found that the combined mechanisms of crack deflection and local deformation after the debonding of the polymer around the particles might be attributed to their improved toughness. Debonding is the separation of fillers from the matrix and could improve the nanocomposite toughness by augmenting the polymer plasticity during deformation, thereby assisting plastic stretching of the polymer ligaments on the nanoparticles.[15–17] For the nanocomposites developed in this study, the direct covalent bonding between the nanoparticles and polymer matrix impeded both the polymer chain and nanoparticle mobility significantly. This lack of mobility could not dissipate the energy during deformation, so cracks were initiated and the nanocomposite eventually failed.[17] In fact, Figure 12 shows that only the neat resin tensile test specimens experienced crazing, whereas the nanocomposites exhibited visible cracks along the gage lengths. Crazing occurs when microcracks and voids form in weak regions during deformation, thereby dissipating stress concentrations and preventing the formation of cracks.[18] Because crazing is one toughening mechanism found in brittle polymers during deformation, its absence in the nanocomposites might further indicate that too strong of an adhesion might not be desirable for mechanical property enhancement. When millions of nanoparticles strongly bonded to the polymer matrix are present, crazing cannot occur; thus, stress concentrations quickly grow toward catastrophic failure. Furthermore, there appears to be an optimum particle size that would maximize the toughening mechanism.[19] That is, a filler that is too small would not initiate craze formation effectively, whereas a particle that is too big would simply act as a stress concentrator. A study of the effects of the nanoparticle size and interfacial bonding on the mechanical properties and fracture mechanisms is being undertaken.

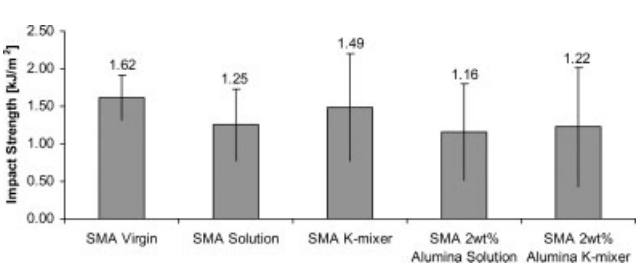

Figure 11 Impact strengths of the SMA neat resins and their nanocomposite counterparts from the solution and melt-compounding methods.

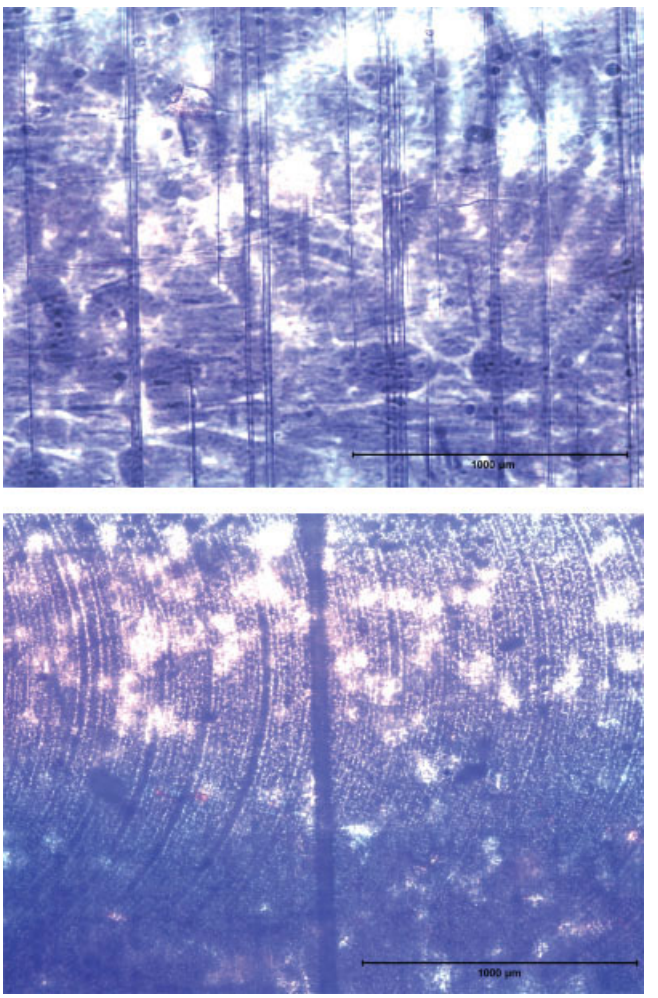

Figure 12 Crazing and cracks (vertical lines) on the SMA neat resin (top) and SMA alumina nanocomposite (bottom). The circular patterns are from the mold surface. [Color figure can be viewed in the online issue, which is available at www.interscience.wiley.com.]

CONCLUSIONS

SMA/alumina nanocomposites were produced via the solution and melt-compounding methods for potential applications in optical products. The nano-

composites were semitransparent to visible light and had improved UV-barrier properties. However, nanoparticle reagglomeration still occurred in the nanocomposite from the solution method, even though good wetting was achieved. On the other hand, the nanoparticle dispersion on the nanocomposite compounded with the high-intensity mixer was excellent. Finally, the nanocomposites did not possess improvements over their neat resin counterparts with respect to the tensile strength, strain at break, or impact strength, although slight enhancements of the moduli were achieved.

The authors acknowledge the help of Scott T. Martin from Thermo Electron Corp. with the injection molding of the specimens.

References

1. Pethrick, R. A. In Thermal and Electrical Conductivity of Polymer Materials; Godovsky, Y. K.; Privalko, V. P., Eds.; Springer-Verlag: New York, 1995; p 81.
2. Vermeesch, I.; Groeninckx, G. J Appl Polym Sci 1994, 53, 1365.
3. Hiemenz, P. C.; Rajagopalan, R. Principles of Colloid and Surface Chemistry; Marcel Dekker: New York, 1997; p 604.
4. Diaz-Quijada, G.; Wayner, D. D. M. Langmuir 2004, 20, 9607.
5. Althues, H.; Palkovits, R.; Rumplecker, A.; Simon, P.; Sigle, W.; Bredol, M.; Kynast, U.; Kaskel, S. Chem Mater 2006, 18, 1068.
6. Caseri, W. Macromol Rapid Commun 2000, 21, 705.
7. Chakraborty, J.; Sarkar, J.; Kumar, R.; Madras, G. Polym Degrad Stab 2004, 85, 555.
8. Madras, G.; Kumar, S.; Chattopadhyay, S. Polym Degrad Stab 2000, 69, 73.
9. Chandra, A.; Gong, S.; Hall, D. C.; Caulfield, D. F.; Yang, H.; Turng, L. S. Polym Compos, to appear.
10. Nussbaumer, R. J.; Caseri, W.; Tervoort, T.; Smith, P. J Nanopart Res 2002, 4, 319.
11. Nussbaumer, R. J.; Caseri, W.; Smith, P.; Tervoort, T. Macromol Mater Eng 2003, 288, 44.
12. Shang, J.; Chai, M.; Zhu, Y. J Solid State Chem 2003, 174, 104.
13. Kemp, T. J.; McIntyre, R. A. Prog React Kinet Mech 2001, 26, 337.
14. Thio, Y. S.; Argon, A. S.; Cohen, R. E.; Weinberg, M. Polymer 2002, 43, 3661.
15. Thio, Y. S.; Argon, A. S.; Cohen, R. E. Polymer 2004, 45, 3139.
16. Shah, D.; Maiti, P.; Jiang, D. D.; Batt, C. A.; Giannelis, E. P. Adv Mater 2005, 17, 525.
17. Lazzeri, A.; Zebarjad, S. M.; Pracella, M.; Cavalier, K.; Rosa, R. Polymer 2005, 46, 827.
18. Nielsen, L. E.; Landel, R. F. Mechanical Properties of Polymers and Composites; Marcel Dekker: New York, 1994; p 302.
19. Arends, C. B. Polymer Toughening; Marcel Dekker: New York, 1996; p 274.